



NUMERICAL AND EXPERIMENTAL INVESTIGATION OF THE VELOCITY FIELD IN FRICTION VENTILATORS

Andreas RENZ¹, Julian PRAB²,
Jörg RIEDEL¹, Olaf NADLER¹, Stefan BECKER¹

¹ FAU Erlangen-Nürnberg, Institute of Process Machinery and Systems
Engineering, Cauerstraße 4, D-91058 Erlangen, Germany

² FAU Erlangen-Nürnberg, Institute for Factory Automation and
Production Systems, Egerlandstraße 7-9, D-91058 Erlangen, Germany

SUMMARY

In an effort to develop a new and simple concept for a decentralized ventilation system with heat recovery a cross flow friction ventilator was investigated. The friction ventilator consists of multiple circular discs which are driven by a motor and are rotating centrally in between the inlet and the outlet duct of the system. The drag between the disc surfaces and the fluid induces countercurrent flows in the ducts while the discs also act as a rotating heat exchanger between the two air flows. In this study, we used Laser Doppler Anemometry to investigate the velocity field at different rotor geometries and operating points. Furthermore, we investigated the secondary currents in the ducts by means of numerical simulations in order to explain the low efficiencies.

INTRODUCTION

The high standards of thermal insulation housing stock, demanded by energy saving regulations (e.g. EnEV 2014 [1]), is limiting the amount of natural air exchange in modern housing stock and therefore leads to problems like structural dampness. To achieve the necessary amount of exchange while still remaining a high energy efficiency centralized and decentralized ventilation systems with heat recovery are becoming increasingly popular.

Decentralized ventilation systems typically consist of three main functional elements: two axial or radial fans for the inlet and the outlet duct and a heat exchanger to transfer heat from the exhaust airflow to the incoming airflow. These decentralized systems ensure the necessary air exchange in single rooms while maintaining high energy efficiency.

A friction ventilator, as described in a patent application [2], combines the three elements into one single functional element. The rotor of a friction ventilator consists of multiple, thin, circular discs which are mounted equidistantly on a driven shaft and with their rotating axis perpendicular to the main flow direction. As shown in Fig. 1, the rotor is mounted in between the inlet and the outlet duct of the ventilation system. At the rotor the two ducts are sealed against each other by contactless sealing elements. The friction between the rotating disc surfaces and the fluid induces two countercurrent airflows (arrows in Fig. 1 show the main flow direction) in the ducts [3]. The rotor additionally serves as a heat exchanger due to the fact that the surface of the rotating discs periodically passes the two air flows. The design is simple, very compact and has a very low overall noise emission.

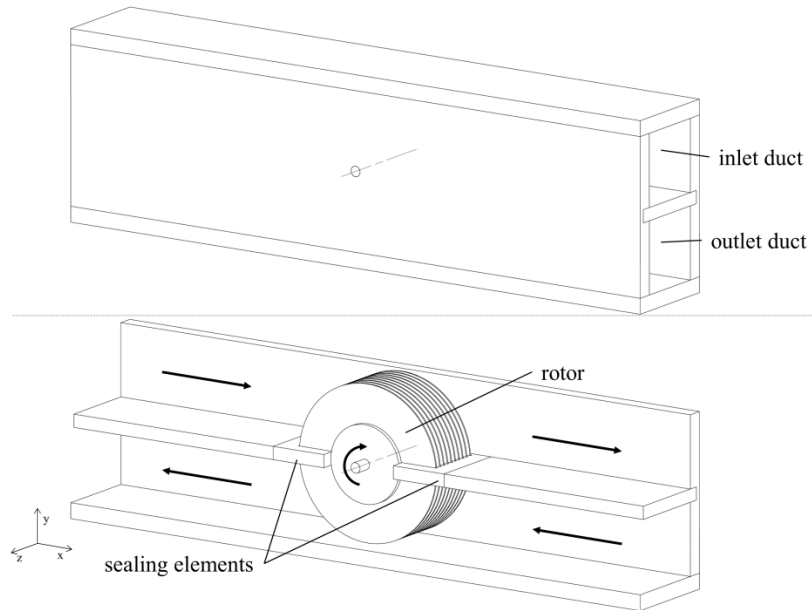


Figure 1: Drawing of a friction ventilator; Lower part: one duct wall and one duct ceiling are hidden.

This study focuses on the investigation of the flow field of the duct section up- and downstream of a friction ventilator as well as the flow field between the rotating discs. Laser Doppler Anemometry (LDA) measurements and numerical simulations were performed for two different ventilator setups.

FRICION VENTILATOR SETUPS

Two friction ventilator setups were investigated which both used the same rotor. In Fig. 2 a drawing of the rotor is given. The rotor consists of ten discs with a diameter of $D = 120$ mm which are separated $\Delta s = 4$ mm by spacers with a diameter of $d = 60$ mm.

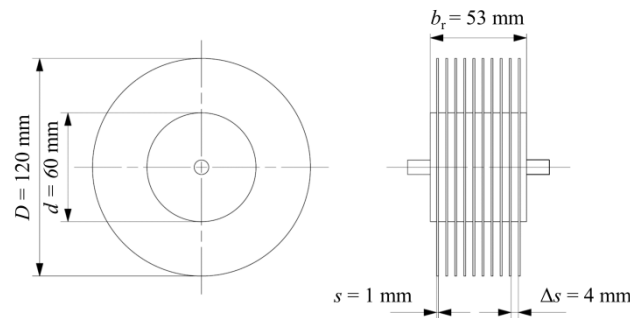


Figure 2: Drawing of investigated rotor.

The difference between the two setups lies in the geometry of the ducts. In Fig. 3 setup A is shown. Here the rotor is fully embedded in the flow through the duct. All of its 20 disc surfaces are in contact with the two main flows in ducts.

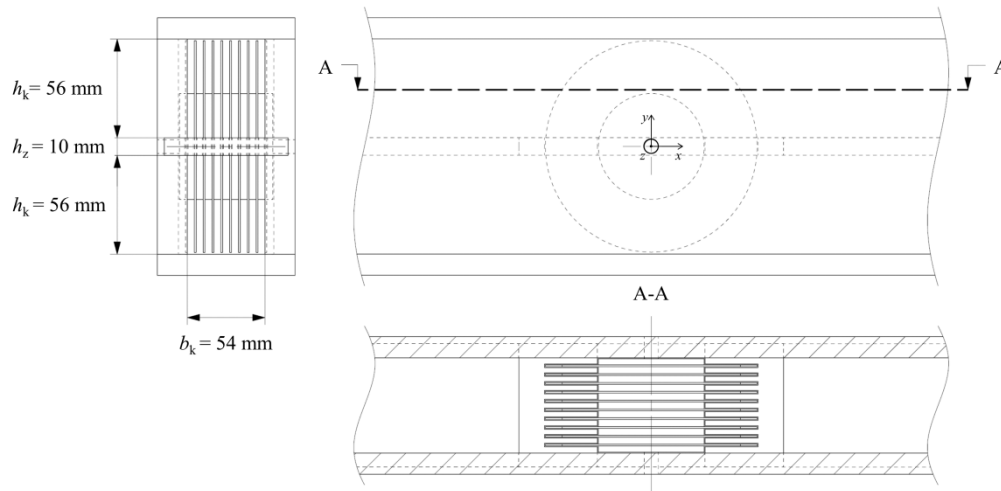


Figure 3: Drawing of the investigated friction ventilator setup A.

Setup B (shown in Fig. 4) features a smaller duct width of $b_k = 44$ mm. Both walls of the ducts have a 5 mm deep indentation in which the outer discs of the rotor are encased. These discs are encased in a way that the inner surfaces of the discs are level with the duct walls. Therefore, only 18 disc surfaces are in contact with the two main flows in ducts.

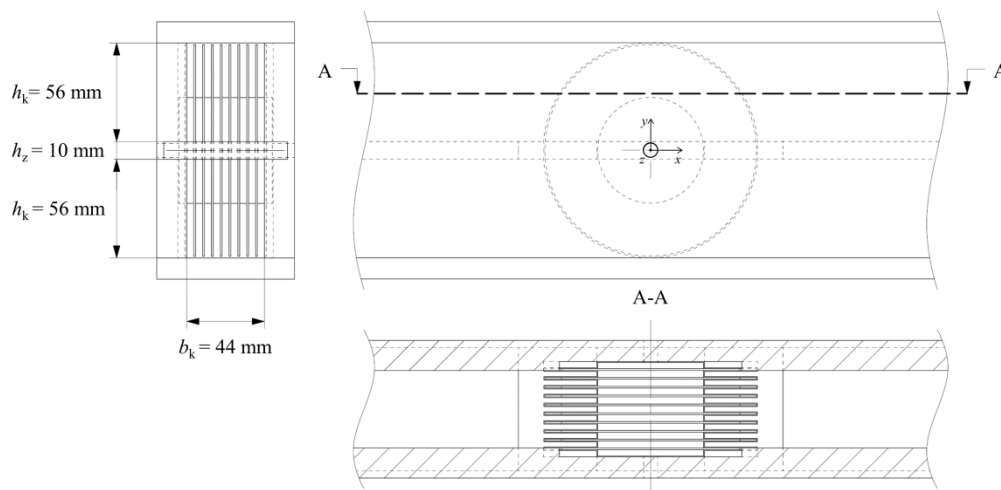


Figure 4: Drawing of the investigated friction ventilator setup B with encased outer discs.

The other main dimensions are the same for the two setups. The distance of the contactless sealing elements to the discs and the hub of the rotor is 0.5 mm all around. The overall duct length is $l = 1000$ mm with the rotor in its center. The upper and lower duct are geometrically identical.

EXPERIMENTAL SETUP

To measure the aerodynamic characteristics and investigate the flow field of the two setups a test rig was used which was designed based on the ISO 5801 [4]. The test rig with its symmetrical two flow courses is shown in Fig. 5. It enables the possibilities to either adjust to an equal mass flow or to an equal volumetric flow in both ducts even if there is a temperature difference between the two flows. To measure the aerodynamic characteristics, the test rig is equipped with an auxiliary fan and volumetric flow meter for each duct to adjust the operating point. Further each duct is connected to a differential pressure transducer to measure the pressure difference between upstream and downstream of the rotor. The rotational speed of the rotor can be precisely adjusted by a servomotor while the torque transmitted to the rotor is measured by a torque meter. Furthermore, four temperature sensors measure the air temperature up- and downstream of the rotor in each duct to calculate the heat recovery rate and additional data (e.g. air density).

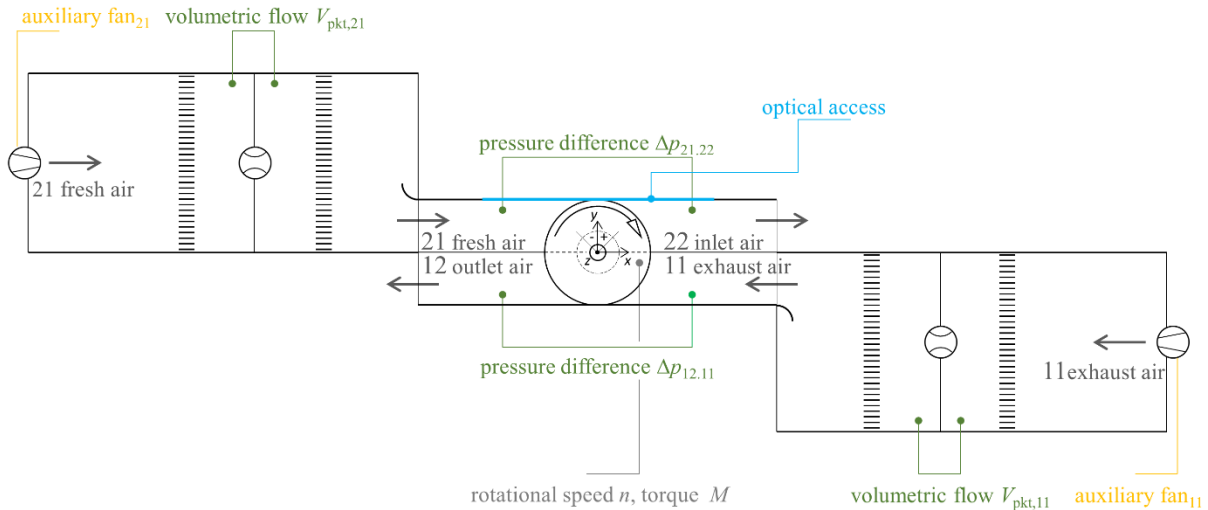


Figure 5: Schematic drawing of used test rig.

The flow field around the rotor and in between the rotor discs was measured with a LDA-system from DANTEC DYNAMICS (Type: Fiberflow). To gain optical access to the flow field a glass window was fitted to the ceiling of the inlet duct (shown in Fig. 5). To acquire the time-averaged part \bar{c}_j and the fluctuating part c_j' of the velocity component c_j in all three dimensions (two dimensions for the measurements in between the discs) measurements from three different LDA-probe angles were performed for each measurement point. The measured velocity values were then calculated according to ALBRECHT [5].

AERODYNAMIC CHARACTERISTICS

The aerodynamic characteristics measured for this study were the characteristic curves and the efficiency for three rotational speeds. In Fig. 6 the characteristic curve for the inlet duct and the efficiency for the system at $n = 4000$ rpm, $n = 6000$ rpm and $n = 8000$ rpm are shown for setup A and setup B.

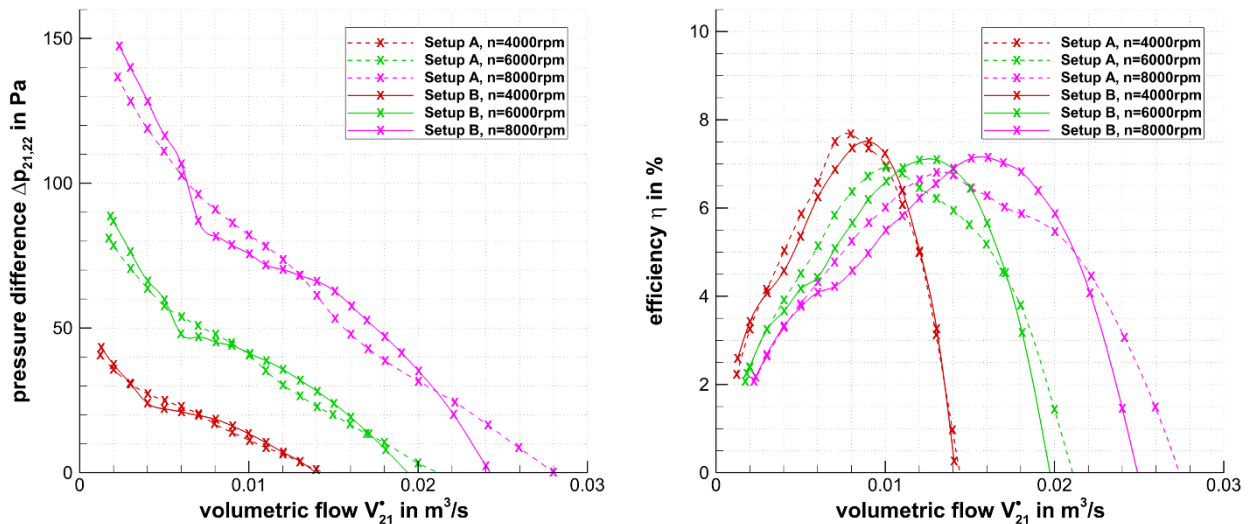


Figure 6: Left: characteristic curve of the inlet duct. Right: efficiency over volumetric flow.

The characteristic curve for the inlet duct shows an almost linear slope for setup A and a slightly more uneven curve for setup B. Overall the results for both setups are very alike although setup B has a smaller overall disc surface area because of the encased outer discs. The overall pressure rise Δp and volumetric flow \dot{V} achieved by the friction ventilator is sufficient for the intended use. The rise in rotational speed n has the same effect on the characteristic curve as in conventional

turbomachinery such as axial or radial fan. With rising speed n the pressure difference Δp and the field of work increase.

The right-hand side of Fig. 6 show the efficiency which is calculated as follows:

$$\eta = \frac{\Delta p_{21,22} \dot{V}_{21} + \Delta p_{12,11} \dot{V}_{11}}{2\pi n M} \quad (1)$$

The overall efficiency η is low for both setups, but similar for different rotational speeds n . There is a certain ratio of mean flow velocity to circumferential velocity at which the efficiency is highest for each setup, unaffected by the rotational speed n . Overall the two setups showed almost similar results although Setup B has a broader range than setup A in which the efficiency is close to maximum.

FLOW FIELD MEASUREMENTS

The focus of the measurements was to investigate the low efficiency and to visualize areas of aerodynamic loss. The flow field was measured at peak efficiency for $n = 6000$ rpm for both setups as this would be the design volume flow rate. For setup A peak efficiency was reached at a volumetric flow of $\dot{V} = 10$ l/s and a mean flow velocity of $\bar{c} = 3.3$ m/s in the duct, for setup B correspondingly at a volumetric flow of $\dot{V} = 13$ l/s and a mean flow velocity of $\bar{c} = 5.3$ m/s in the duct. In the following the two setups will be compared side by side to show the difference of the overall flow field. Because of the different mean flow velocity, the absolute velocity values are not comparable.

In Fig. 7 the measuring planes for setup A are shown. Here two xy -planes (blue in Fig. 7) were measured, one close to the duct wall and a second plane in the duct's center. Two yz -planes (green in Fig. 7) were measured to compare the flow field 100 mm upstream and downstream of the rotor. Furthermore, the flow field in between the discs was investigated in three planes in radial direction of the rotor axis (red in Fig. 7). The measuring planes for setup B were chosen accordingly.

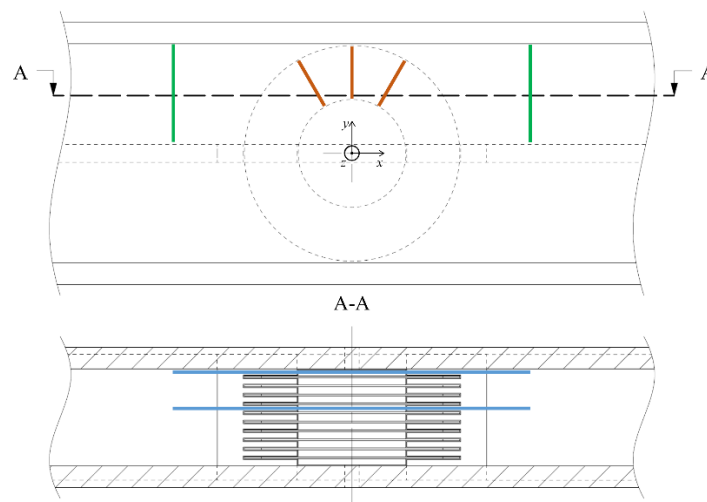


Figure 7: LDA measuring planes in setup A.

To compare the setups each Figure contains the results of setup A and setup B. First (Fig.8-10) the results for the time-averaged velocity fields are shown for the above mentioned position, followed (Fig. 11 and 12) by the results for the measurement of the turbulent kinetic energy k in the planes. The arrows in the plots represent the time-averaged velocity components \bar{c} in the shown measuring plane with their velocity values normalized by a given unity vector. The contour plots give additional information like the turbulent kinetic energy k .

Fig. 8 and Fig. 9 show an ordinary flow field for a duct flow upstream of the rotor with little secondary flows. The rotating ventilator is not influencing the upstream flow in the investigated operating points. However, we can see a difference in the downstream flow for the two setups.

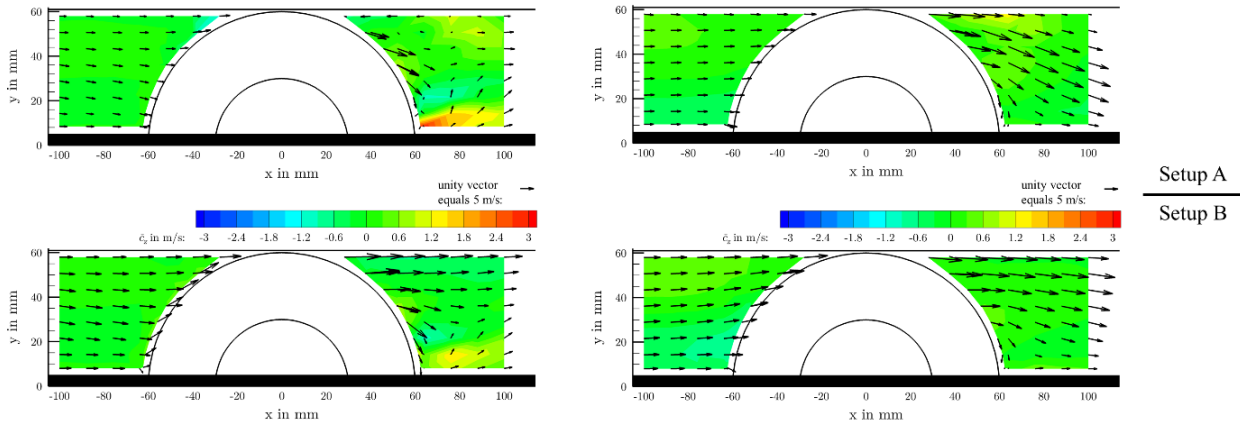


Figure 8: Time-averaged velocity component \bar{c}_{xy} (arrow) in the xy -plane with the time-averaged velocity component \bar{c}_z (contour). Left plots: close to the duct wall; Right plots: duct center.

In Fig. 8 the flow fields of setup B for the two measuring planes show only minor differences to one another. For setup A there is a difference between the two planes as the velocity values for the component \bar{c}_{xy} close to the duct are low und undirected compared to the duct's center, even backflow can be observed. The main flow direction in the duct's center downstream of the rotor seems to turn towards the duct floor for setup A, whereas the main flow direction of setup B follows the direction of the duct. This is also observable in Fig. 9 where the highest time-averaged velocity \bar{c}_x for setup A can be seen in the middle of the duct while the maximum for setup B is close to the duct ceiling. Crossflow can be observed for both setups in the lower part close to the duct wall.

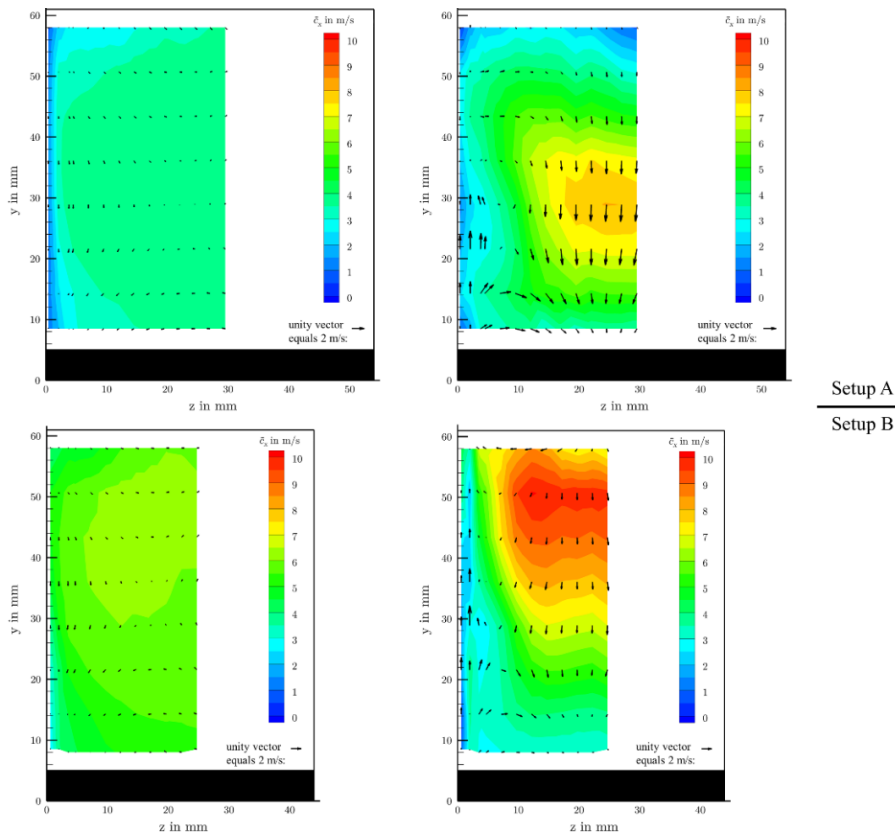


Figure 9: Time-averaged velocity component \bar{c}_{xz} (arrow) in the yz -plane with the time-averaged velocity component \bar{c}_x (contour). Left plots: 100 mm upstream of the rotor; Right plots: 100 mm downstream of the rotor. The duct wall is located at $z = 0$ (outer left side of each picture).

It seems that the encased outer discs of setup B create a more uniform flow field directly downstream of the rotor. In Fig. 10 the influence of the encasement on the flow field is even more pronounced. For setup B the flow through three different disc channels is almost uniform whereas the flow between the outer discs and the duct wall for setup A shows large areas with backwards flow. Overall the measurement between the discs also showed that a large part of the flow through the rotor is only mildly affected by the rotating discs and that a reduction in discs spacing could be beneficial.

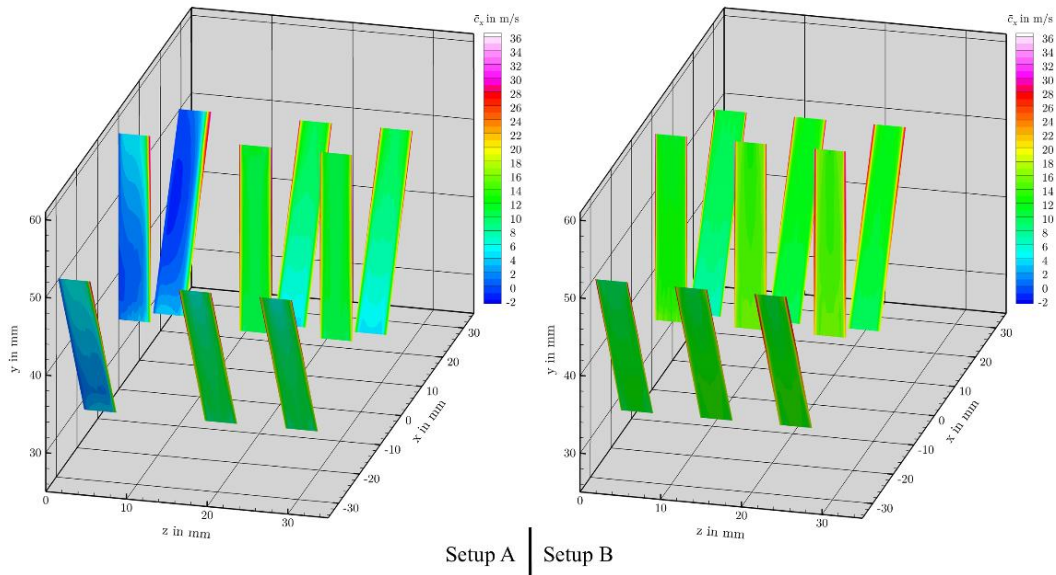


Figure 10: Time-averaged velocity component \bar{c}_x (contour) in three discs channels. $z = 0$ equals the duct wall.

The results for the measurement of the turbulent kinetic energy k in two xy -planes are shown in Fig. 11. In the upstream flow field of the rotor the turbulent kinetic energy k tends to zero for both setups. Downstream of the rotor, however, there is a big difference, especially close to duct wall. Here setup B shows only increased turbulent kinetic energy k closely behind the rotor, whereas setup A shows high values over a large area. In the center of the duct the differences are not as big, although an area with high values of k and low flow velocity \bar{c}_{xy} can be observed close to the duct ceiling of setup A. This could indicate an area of recirculation further downstream.

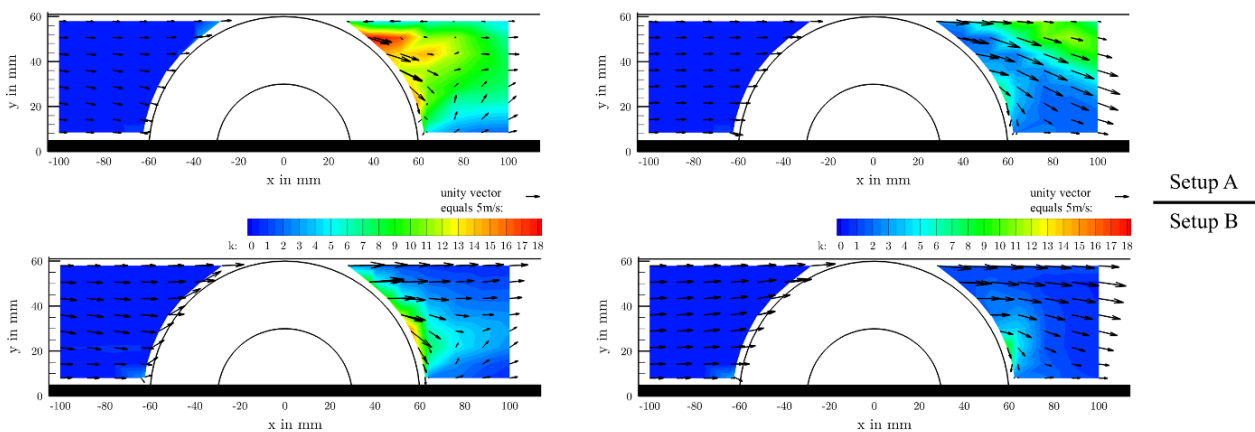


Figure 11: Time-averaged velocity component \bar{c}_{xy} (arrow) in the xy -plane with the turbulent kinetic energy k (contour).
 Left plots: close to the duct wall; Right plots: duct center.

Fig. 12 confirms the observations made above. The value of k tends towards zero for the flow upstream and slightly elevated level for the yz -planes in setup B downstream of the rotor. Solely the downstream yz -plane of setup A shows high values over a large area.

Overall the measurements of the flow field showed that the encasement of the outer discs (setup B) had only positive effects on the flow field in the measured area. The flow downstream of the rotor was much more uniform and showed greatly reduced levels of turbulent kinetic energy k .

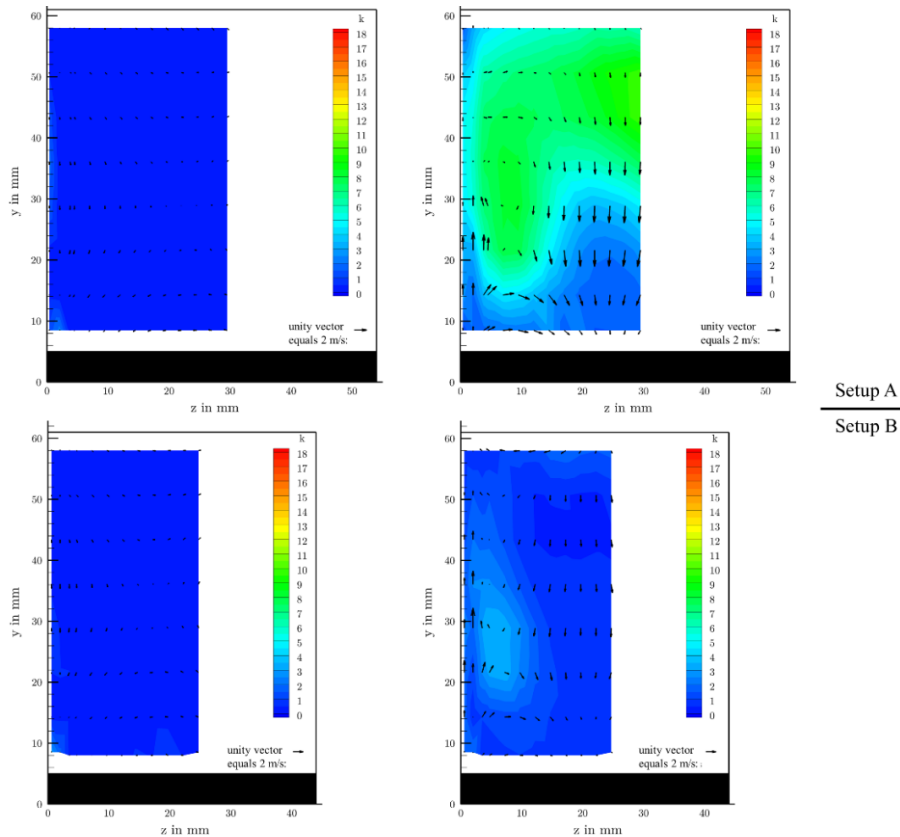


Figure 12: Time-averaged velocity component \bar{c}_{xz} (arrow) in the yz -plane with the turbulent kinetic energy k (contour).
Left plots: 100 mm upstream of the rotor; Right plots: 100 mm downstream of the rotor.
The duct wall is located at $z = 0$ (outer left side of each picture).

The flow through the discs seemed to benefit most of the encased outer discs as backward flows through the disc channels were eliminated. Why these improvements didn't affect the overall efficiency is to be investigated as the resistance of the encased rotating discs is too small to have a considerable effect. It's possible that there are large areas of recirculation downstream of the measured area. This will be the focus of further measurements.

For the carried out measurements the experimental uncertainty was estimated in accordance with the guide to the expression of uncertainty in measurements (GUM) [6]. The expanded uncertainties for the volumetric flow \dot{V} ($U_{\dot{V}} = 0,81\%$), the pressure rise Δp ($U_{\Delta p} = 0,75\%$), the overall efficiency η ($U_{\eta} = 0,79\%$) and the time-averaged velocity components \bar{c}_i ($U_{\bar{c}_x} = 0,28\%$, $U_{\bar{c}_y} = 1,47\%$, $U_{\bar{c}_z} = 0,28\%$) were evaluated using a coverage factor of 2 which gives a level of confidence of 95 %.

SIMULATION SETUP

Measurements are well suited for examining a large variety of parameter setups – such as rotational velocity, pressure difference and volume flux – as long as the geometry of rotor and channel do not change. As different geometries need to be manufactured simulations have been used to investigate the influence of different disc spacing of the rotor. Therefore, the setup A was investigated numerically and compared to the measurements. The model was first simplified to one single side of a disc rotating in the corresponding part of a channel with symmetry boundary conditions on the sides as shown in Fig. 13 (middle). Using only this part of the model, the computational effort was

drastically reduced. As this approach was known to yield good results for the nominal point of the ventilator for different hub diameters [7] it was of interest to evaluate the effect of the symmetry boundary conditions on the parts of the characteristic curve of very low and very high volume fluxes. As the simulation of only one side of a disc can't account for crossflows, a simulation of a domain including five discs and thus half of the entire channel was created.

All simulations were run using a $k-\omega$ -SST model within ANSYS CFX®. For both domains – referred to as *single disc* and *half channel* – grid dependency studies were carried out for unstructured and block structured meshes in order to minimize errors resulting from coarse grids. Furthermore, the results for single disc simulations and half channel simulations were compared with the experiments for the entire characteristic curve in order to validate the simulations. From these validations, the most suitable setup was chosen for simulations of characteristic curves of rotors with different disc spacing that were not manufactured.

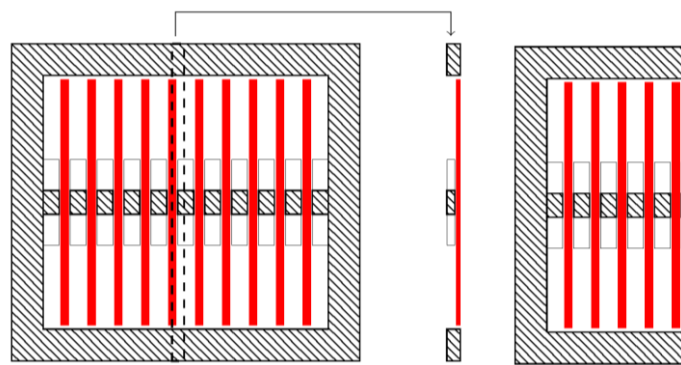


Figure 13: Crosssection of the friction ventilator (left), simplified domain including one single disc (middle) and half channel (right).

Validation

In order to minimize the uncertainties in the simulations stemming from insufficient resolution and boundary conditions that are not able of capturing all effects of the flow three different methods of validation have been applied. Namely these were comparisons for different mesh resolutions, different domain sizes and different mesh types.

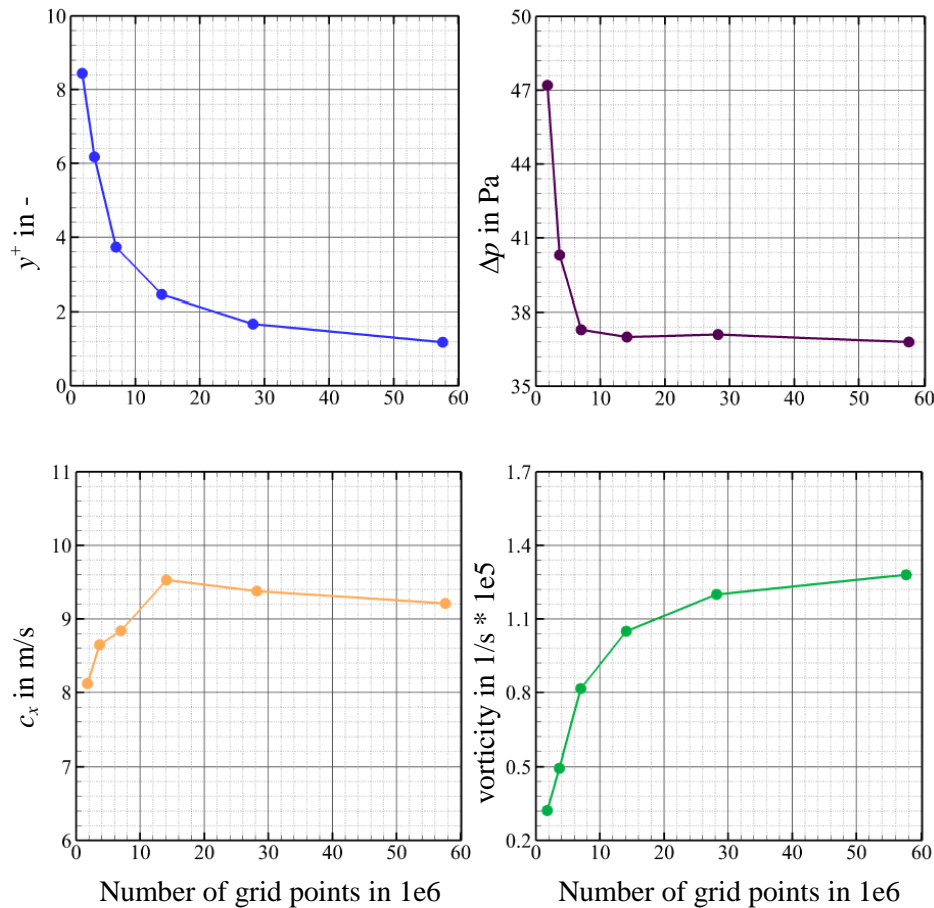


Figure 14: Results of the grid dependency study of the block structured mesh for the single disc.

The results of the grid dependency study are exemplarily shown in Fig. 14 for the block structured mesh. It can be seen that the results for pressure difference Δp and velocity in main flow direction c_x do not change dramatically for meshes with 14e6 elements. Richardson extrapolation for the meshes consisting of 3.6e6, 7.0e6 and 14.1e6 elements confirms that the discretization error is less than 1 % for the mesh of 14.1e6 elements. For this reason, this mesh was chosen for the block structured approach. The same was done for the unstructured mesh yielding an optimal mesh consisting of 14.9e6 elements.

Fig. 15 shows the comparison of the simulation of a single disc (left) and the half channel (right) for block structured and unstructured meshes. It can be seen that in unstructured mesh overestimates the performance of the ventilator in case of simulating one single disc. The block structured mesh performs slightly better for low and medium volume fluxes but also overestimates the maximum pressure jump for high volume fluxes. It is very likely that crossflows might appear in the case of high volume fluxes that can't be captured by the symmetry boundary condition. The comparison of simulation and experiment for the half channel (Fig. 15, right) shows, that both the unstructured and the block structured meshes lead to very good results. While the unstructured grid underestimates the pressure jump for the entire volume flux region investigated, the block structured grid has very little differences to the experimental values for volume fluxes higher than 0.012 m³/s but overestimates the performance for lower volume fluxes. Calculating the residual sum of squares of the differences between the simulated and measured points of the characteristic curves leads to a value of 645 Pa² for the block structured mesh and 687 Pa² for the unstructured mesh. This leads to an average root mean square error of 8.03 Pa for the block structured and 8.29 Pa for the unstructured mesh which shows that both simulations are capable of representing the characteristic curve of the ventilator. Still the block structured mesh shows a slight better performance and was thus used for the investigation of different geometrical setups.

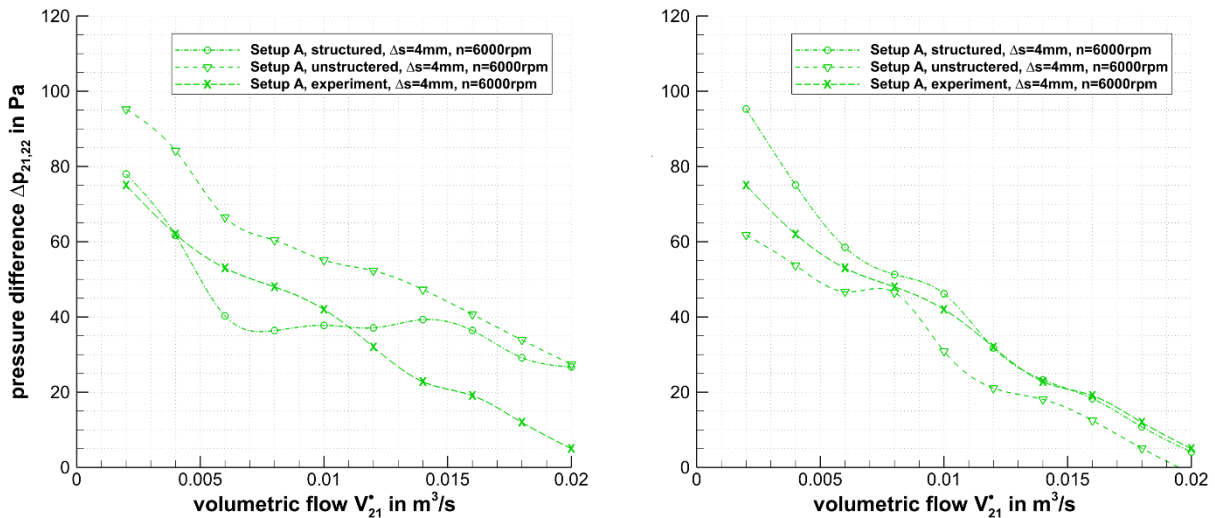


Figure 15: Comparison of characteristic curves for simulations of a single disc (left) and half channel (right) for lock structured and unstructured meshes with the experiment.

Investigation of different geometrical setups

As the validation showed the best results for the block structured mesh this approach was used to simulate the characteristic curves for two more geometrical setups that have not been manufactured. In this study, different disc spacing Δs of 3 mm and 5 mm have been investigated and compared to the existing results for 4 mm. The characteristic curves shown in Fig. 16 unveil that on the one hand the maximum pressure difference Δp can be slightly increased by using lower disc spacing but on the other hand this drastically reduces the maximum volume flux that can be delivered.

This behavior changes for the case of 5 mm disc spacing. Here, it is not possible to obtain high pressure differences even for low volume fluxes, but the maximum volume flux to be delivered is much higher than for 4 mm disc spacing.

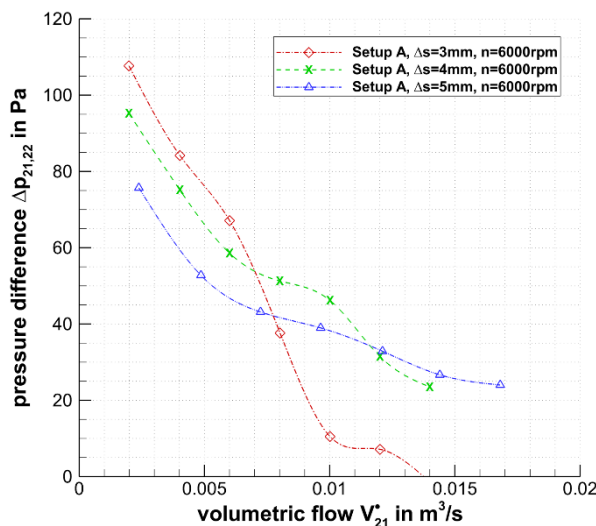


Figure 16: Simulated characteristic curves for different geometric setups that have not been manufactured.

This behavior is also present for different rotational speeds, where the characteristic curves are shifted to higher pressure differences for higher rotational speeds and vice versa whereas the shape of the curves stays almost unaffected of the rotational speed and is thus more bound to the geometry

of the rotor rather than the state of operation. This means that special attention has to be paid to the use of higher disc spacing, as the gradient $\Delta p / \Delta \dot{V}$ rises over the entire curve. Therefore, the ventilator is more likely to be run in unstable operating points which has to be considered when using such a ventilator as a decentralized ventilation system.

CONCLUSION

A friction ventilator that is meant to be used as a decentralized ventilation system with heat recovery has been investigated in experiments and numerically. The measurements of the characteristic curves showed the general suitability of both investigated setups for its intended use. Solely the overall hydrodynamic efficiency was lower than expected. LDA-measurements of the flow field up- and downstream of the rotor showed advantages for setup B as the flow for this setup was much more uniform and the overall turbulence intensity decreased. Nevertheless, these observations didn't result in increased efficiencies. Based on the gathered information, it is likely that there are areas of recirculation further downstream of the rotor which lead to high aerodynamic losses. These areas will be the focus of further flow measurements. In order to investigate the performance of different geometries of the rotor, numerical simulations have been carried out that were validated with the experiments of setup A. It was shown that the complex flow field can't be represented properly by the simulation of the flow around one single disc with symmetry boundary conditions as it is not possible to capture cross flows with this setup. Therefore, additional simulations of the half channel including five discs have been carried out with block structured and unstructured meshes. Both mesh types performed well and captured the overall characteristic curves with slightly better results for the block structured mesh. On the basis of these results different geometrical setups have been investigated that showed that lower disc spacing leads to steeper characteristic curves with higher maximum pressure differences and lower maximum volume fluxes.

BIBLIOGRAPHY

- [1] Bundesministerium der Justiz und für Verbraucherschutz – *Verordnung über energiesparenden Wärmeschutz und energiesparende Anlagentechnik bei Gebäuden*, **2007**
- [2] C. Bakeberg, M. Becher, S. Becker, R. Pauer, and E. Schlücker – *Vorrichtung zur Förderung zweier Fluidströme*, Patent application WO 2015/007351 A1, **2015**
- [3] S. Becker, T. Beede, and R. Pauer – *Entwicklung eines neuartigen Gerätes zur dezentralen Be- und Entlüftung von Räumen mit Wärmerückgewinnung*, Strömungstechnische Tagung 2014, **2014**
- [4] DIN EN ISO 5801 – *Industrial fans - Performance testing using standardized airways*, Beuth Verlag, **2007**
- [5] H. Albrecht – *Laser-Doppler-Strömungsmessung*, Bd. 2, Akademie Verlag, **1986**
- [6] ISO/IEC Guide 98-3:2008-09 – *Uncertainty of measurement – Part 3: Guide to the expression of uncertainty in measurement (GUM:1995)*, Beuth Verlag, **2008**
- [7] J. Praß, A. Renz, J. Weber, J. Franke, S. Becker – *Numerical Investigation of a Friction Ventilator for Different Geometrical Setups*, Advanced Engineering Forum vol. 19, pp. 35-42, **2016**